catalysts

MDPI

Supplementary Matterials

Selective and Efficient Reduction of Nitrate to Gaseous Nitrogen from Drinking Water Source by UV/Oxalic Acid/ Ferric Iron Systems: Effectiveness and Mechanisms

Zhiyuan Shi [1], Falu Wang [2,3,4], Qian Xiao [2,3,*], Shuili Yu [2,3,*] and Xingli Ji [2,3]

[1] SIIC Environment Holdings Ltd., Shanghai 200021, China; shizhiyuan@siic.com
[2] State Key Laboratory of Pollution Control and Resource Reuse, College of Environmental Science and Engineering, Tongji University, Siping Campus, Shanghai 200092, China; wangfalu@smedi.com (F.W.); jixingli@tongji.edu.cn (X.J.)
[3] Shanghai Institute of Pollution Control and Ecological Security, Siping Campus, Shanghai 200092, China
[4] Shanghai Municipal Engineering Design Institute (Group) Co., Ltd., Shanghai 200092, China
* Correspondence: 2015xiaoqian@tongji.edu.cn (Q.X.); ysl@tongji.edu.cn (S.Y.); Tel./Fax: +86-21-6598-2708 (Q.X. & S.Y.)

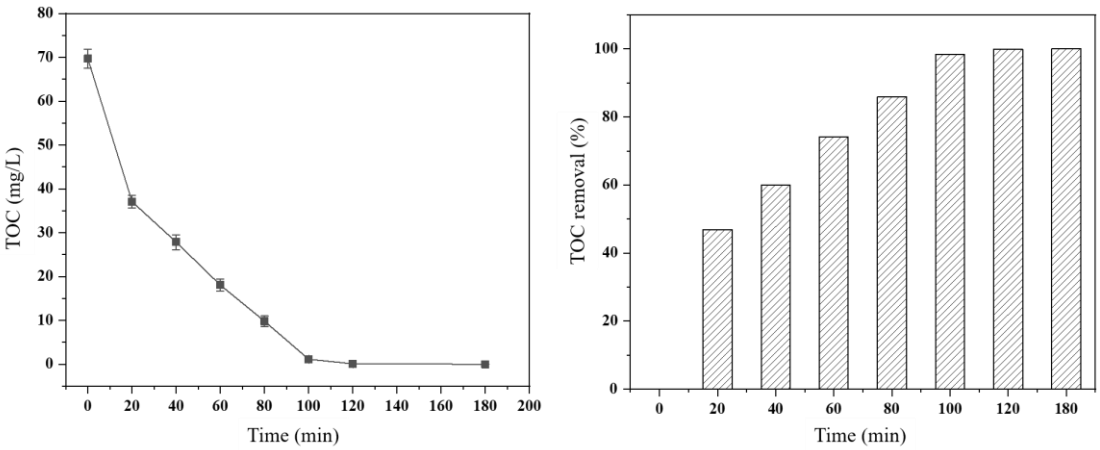

Figure S1. Mineralization of oxalic acid in the UV/$C_2O_4^{2-}$/Fe^{3+} systems. Experimental conditions: $[NO_3^-]_0$ = 60 mg/L, $[C_2O_4^{2-}]_0$ = 3 mM, $[Fe^{3+}]_0$ = 0.05 mM, I_0 = 10.2 mW/cm² (wavelength = 365 nm), $[DO]_0$ = 0.5 ± 0.1 mg/L, $pH_{ini.}$ = 7.0 ± 0.2, and T = 25 ± 0.5 ºC. Error bars represent the standard deviation from three times experiments. Error bars smaller than symbols are not visible.

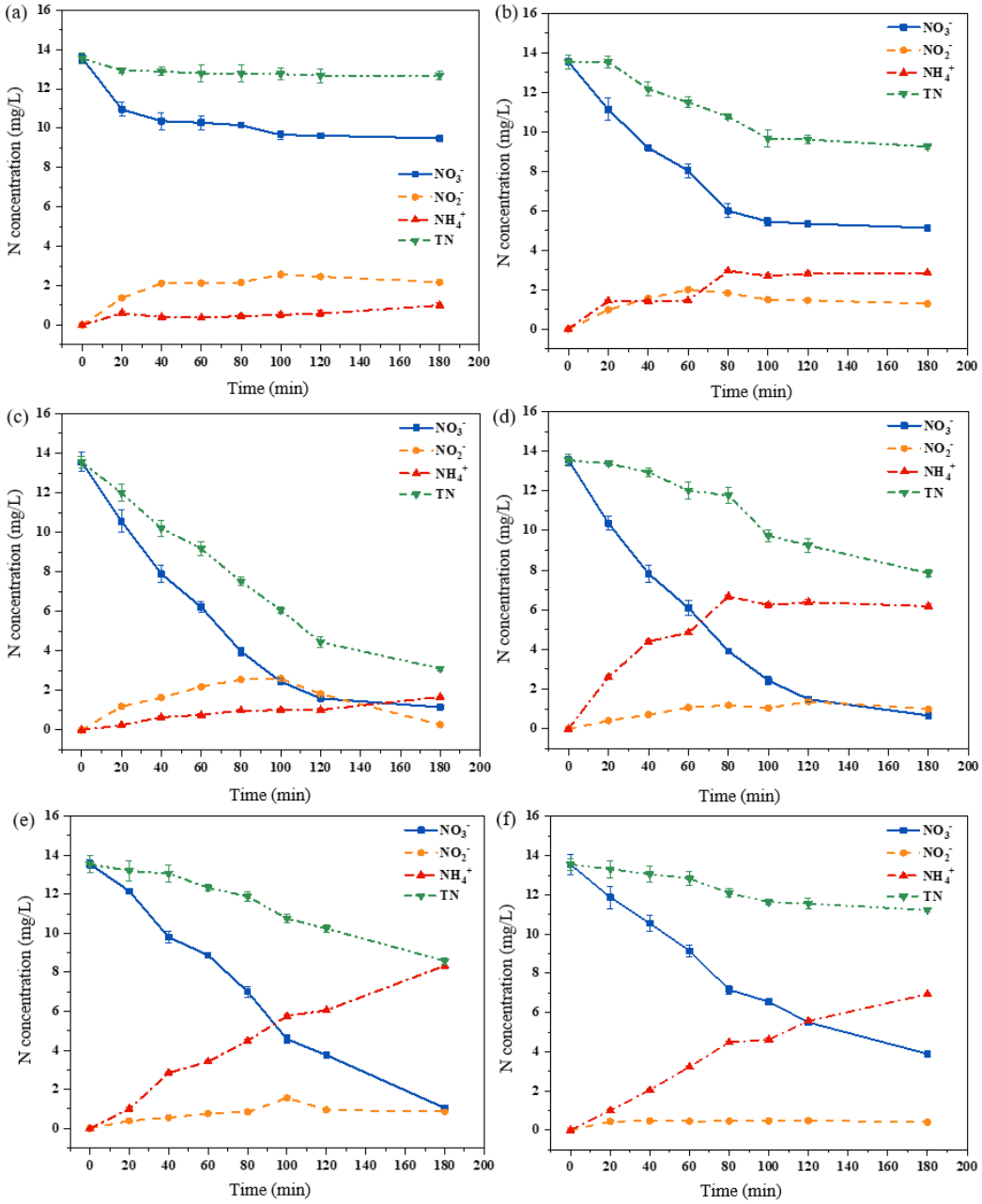

Figure S2. Formation of primary products at different dosage of oxalate acids during reduction of NO_3^- in the UV/$C_2O_4^{2-}$/Fe^{3+} systems. Experimental conditions: $[NO_3^-]_0$ = 60 mg/L, $[C_2O_4^{2-}]_0$ = 1, 2, 3, 4, 5, 6 mM in (a), (b), (c), (d), (e), and (f), respectively, $[Fe^{3+}]_0$ = 0.05 mM, I_0 = 10.2 mW/cm^2 (wavelength = 365 nm), $[DO]_0$ = 0.5 ± 0.1 mg/L, $pH_{ini.}$ = 7.0 ± 0.2, and T = 25 ± 0.5 ºC. Error bars represent the standard deviation from three times experiments. Error bars smaller than symbols are not visible.

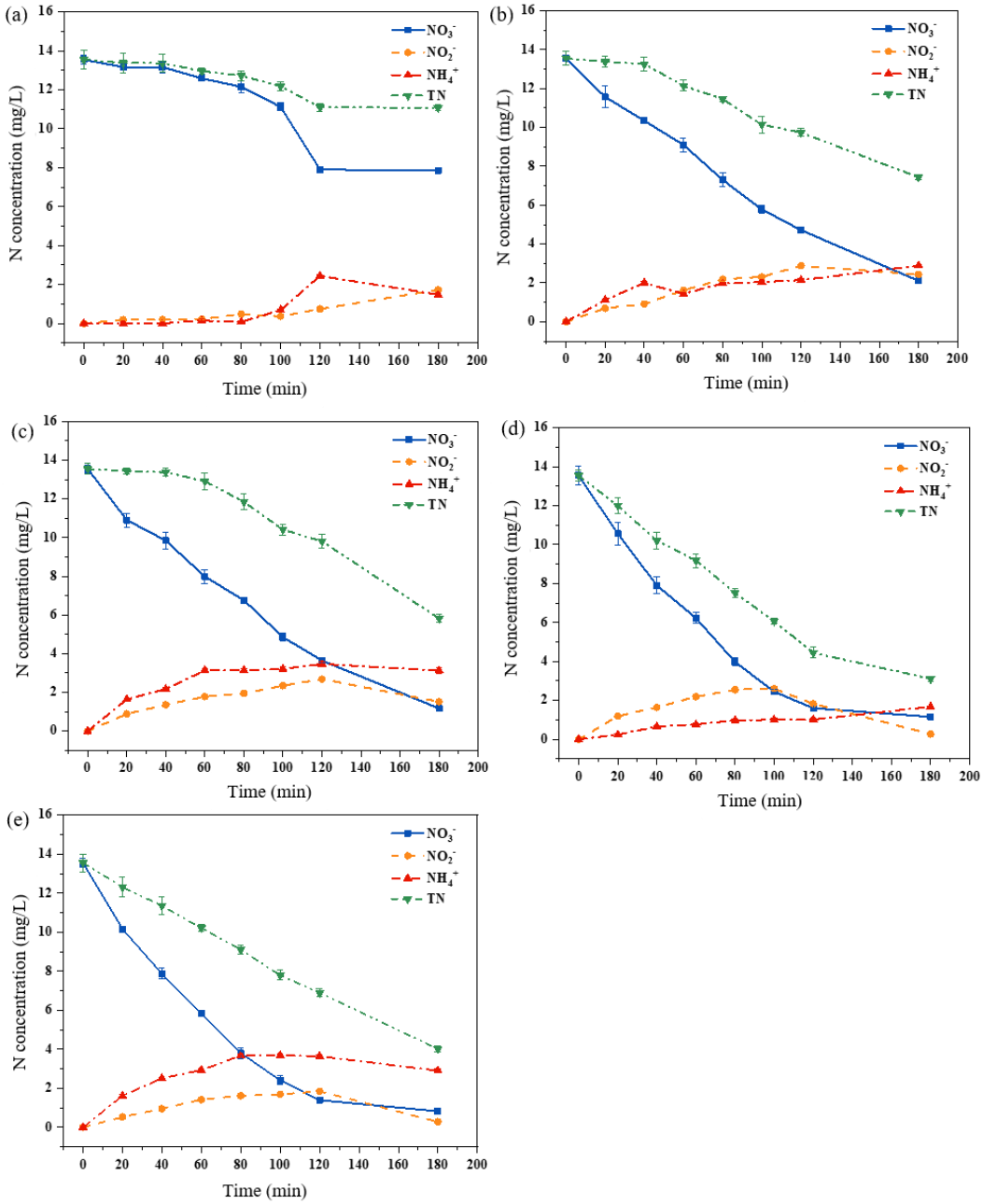

Figure S3. Formation of primary products at different initial Fe^{3+} levels during reduction of NO_3^- in the UV/$C_2O_4^{2-}$/Fe^{3+} systems. Experimental conditions: $[NO_3^-]_0$ = 60 mg/L, $[C_2O_4^{2-}]_0$ = 3 mM, $[Fe^{3+}]_0$ = 0, 0.017, 0.025, 0.05, and 0.1 mM, respectively, in (a), (b), (c), (d), and (e), I_0 = 10.2 mW/cm^2 (wavelength = 365 nm), $[DO]_0$ = 0.5 ± 0.1 mg/L, $pH_{ini.}$ = 7.0 ± 0.2, and T = 25 ± 0.5 ºC. Error bars represent the standard deviation from three times experiments. Error bars smaller than symbols are not visible.

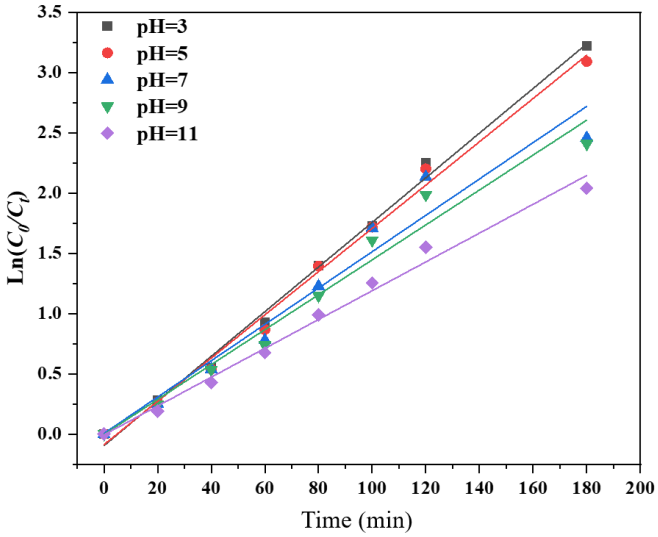

Figure S4. The ln(C_0/C) value versus reaction time at various solution pH in the UV/$C_2O_4^{2-}$/Fe^{3+} systems. Experimental conditions: [NO_3^-]$_0$ = 60 mg/L, [$C_2O_4^{2-}$]$_0$ = 3 mM, [Fe^{3+}]$_0$ = 0.05 mM, power of the UV-M = 500 W, [DO]$_0$ = 0.5 ± 0.1 mg/L, and T = 25 ± 0.5 ºC. Error bars represent the standard deviation from three times experiments. Error bars smaller than symbols are not visible.

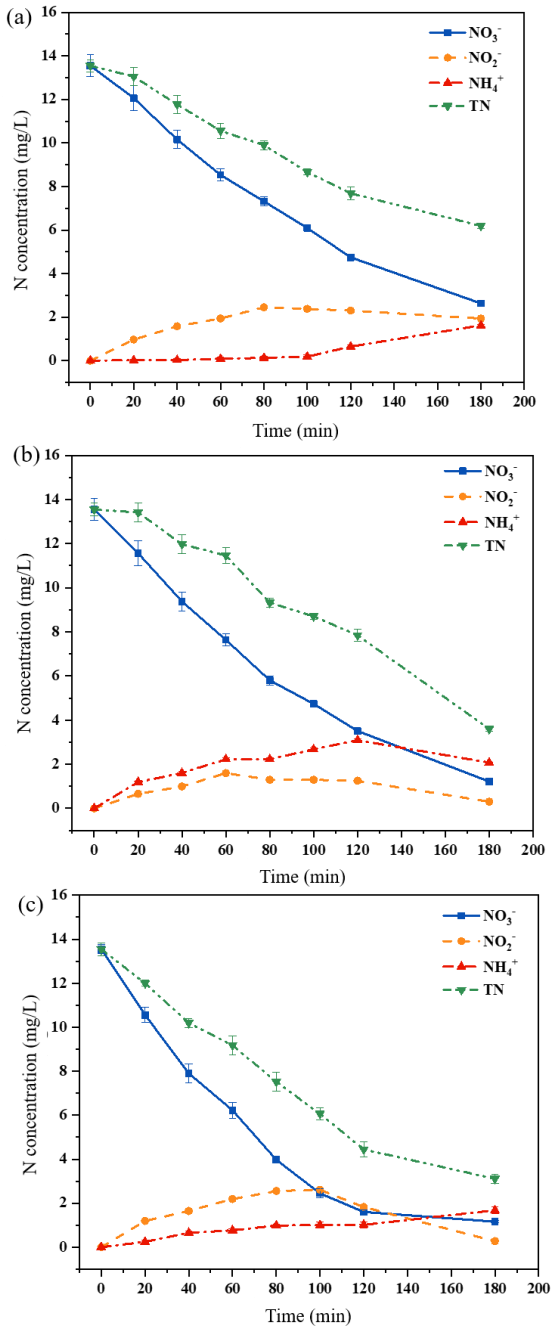

Figure S5. Formation of primary products at different UV lamp power during reduction of NO_3^- in the UV/$C_2O_4^{2-}$/Fe^{3+} systems. Experimental conditions: $[NO_3^-]_0$ = 60 mg/L, $[C_2O_4^{2-}]_0$ = 3 mM, $[Fe^{3+}]_0$ = 0.05 mM, power of the UV-M = 100, 300, and 500 W, respectively in (a), (b), and (c), $[DO]_0$ = 0.5 ± 0.1 mg/L, $pH_{ini.}$ = 7.0 ± 0.2, and T = 25 ± 0.5 ºC. Error bars represent the standard deviation from three times experiments. Error bars smaller than symbols are not visible.

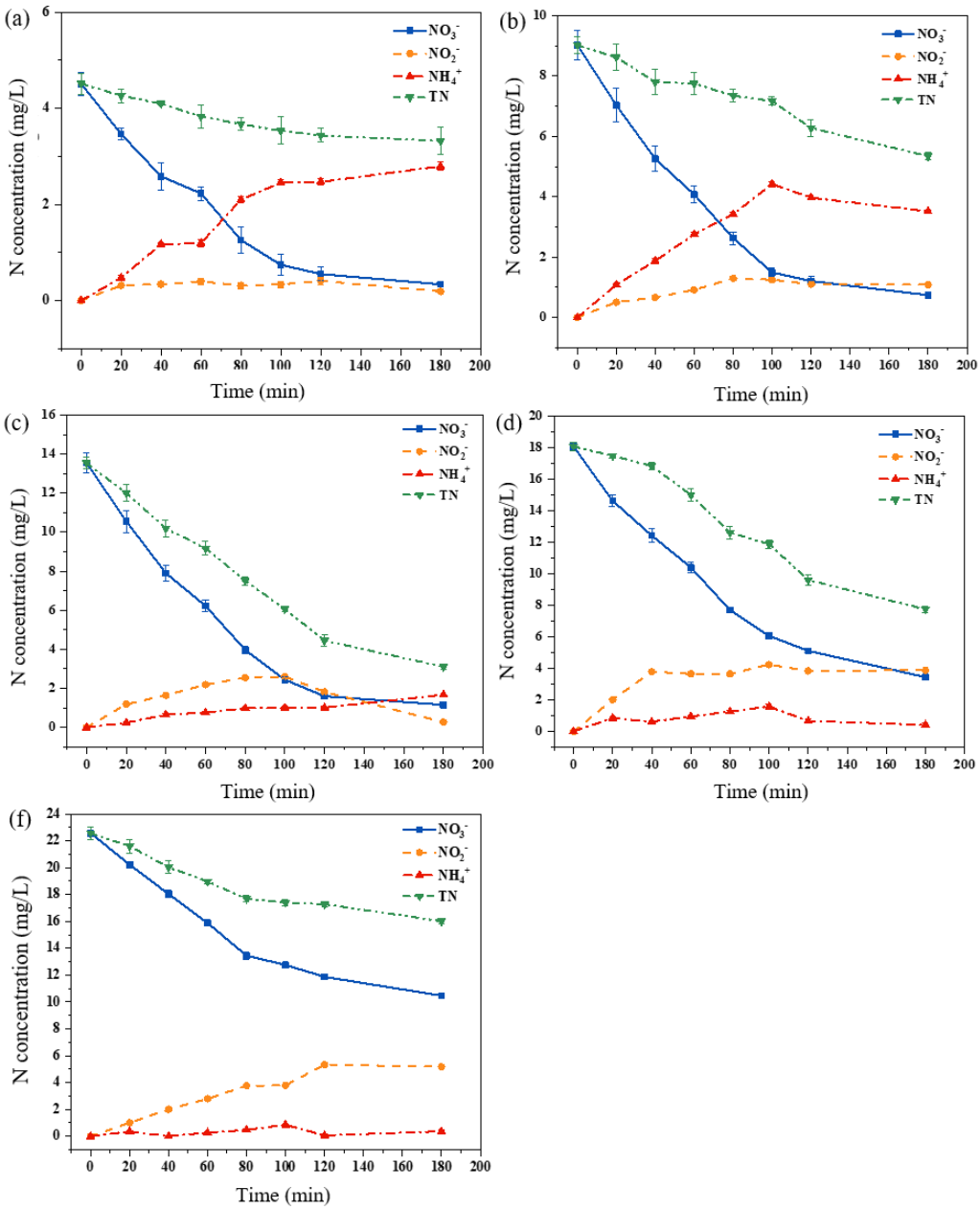

Figure S6. Formation of primary products at various initial NO_3^- levels during reduction of NO_3^- in the UV/$C_2O_4^{2-}$/Fe^{3+} systems. Experimental conditions: $[NO_3^-]_0$ = 20, 40, 60, 80, and 100 mg/L, respectively, in (a), (b), (c), (d), and (e), $[C_2O_4^{2-}]_0$ = 3 mM, $[Fe^{3+}]_0$ = 0.05 mM, the UV-M power = 500 W, $[DO]_0$ = 0.5 ± 0.1 mg/L, $pH_{ini.}$ = 7.0 ± 0.2, and T = 25 ± 0.5 ºC. Error bars represent the standard deviation from three times experiments. Error bars smaller than symbols are not visible.

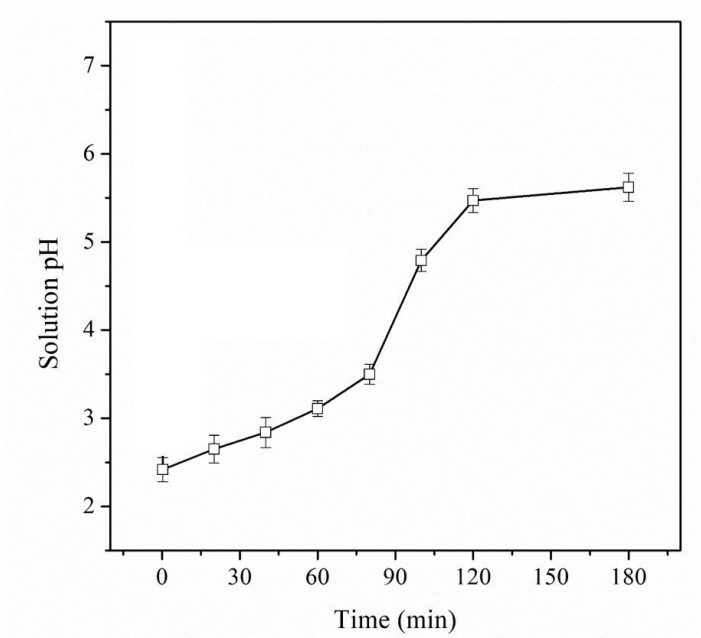

Figure S7. The variation of solution pH with time in the UV/$C_2O_4^{2-}$/Fe^{3+} systems. Experimental conditions: $[NO_3^-]_0$ = 60 mg/L, $[C_2O_4^{2-}]_0$ = 3 mM, $[Fe^{3+}]_0$ = 0.05 mM, I_0 = 10.2 mW/cm^2 (wavelength = 365 nm), $[DO]_0$ = 0.5 ± 0.1 mg/L, and T = 25 ± 0.5 ºC. Error bars represent the standard deviation from three times experiments.

Table S1. The characteristics of simulated groundwater.

Water quality indexes	Level (mg/L)	Water quality indexes	Level (mg/L)
NO_3^-	124	Mg^{2+}	48
HCO_3^-	122	Cl^-	142
K^+	78	SO_4^{2-}	384
Na^+	184	TOC	3.0
Ca^{2+}	40		

Table S2. Kinetic parameters of NO_3^- reduction at various Fe^{3+} levels.

Fe^{3+} level (mM)	First-order reaction kinetic equations	k	R^2
0	y=0.00182x-0.01802	0.002	0.862
0.017	y=0.01022x-0.11464	0.010	0.972
0.025	y=0.01321x-0.17208	0.013	0.953
0.05	y=0.01507x-0.00628	0.015	0.951
0.1	y=0.01671x-0.03667	0.017	0.973

Table S3. Kinetic parameters of NO_3^- reduction at different initial solution pH.

$pH_{ini.}$	First-order reaction kinetic equations	k	R^2
3	y=0.01851x-0.09488	0.01851	0.99394
5	y=0.01794x-0.08683	0.01794	0.99196
7	y=0.01507x+0.00628	0.01507	0.95144
9	y=0.01448x-0.00226	0.01448	0.96644
11	y=0.01195x-0.00559	0.01195	0.98780

Table S4. Kinetic parameters of NO_3^- reduction at different UV light intensity.

Power of UV-M (W)	First-order reaction kinetic equations	k	R^2
100	y=0.0092x-0.06888	0.009	0.992
300	y=0.00992x-0.06525	0.010	0.993
500	y=0.01507x-0.00628	0.015	0.951